PROCEEDINGS, Thirty-Sixth Workshop on Geothermal Reservoir Engineering
Stanford University, Stanford, California, January 31 - February 2, 2011
SGP-TR-191

A THREE-DIMENSIONAL STOCHASTIC FRACTURE NETWORK MODEL FOR GEOTHERMAL RESERVOIR STIMULATION

Xiaonan Wang, Ahmad Ghassemi

Department of Petroleum Engineering, Texas A&M University
College Station, TX, 77843
e-mail: ahmad.ghassemi@pe.tamu.edu

ABSTRACT

An important issue in geothermal resource development is engineering a fractured reservoir and predicting its future performance. For reaching this objective, numerical modeling of flow and deformation of fractured rock is necessary. This can be achieved by developing deterministic fracture models or models that utilize discrete fracture networks. This study focuses on utilizing stochastic fracture networks to simulate flow in fractured rock and to assess the mechanical rock mass response to stress variations caused by injection/production. A finite element numerical model of fracture network with stochastic description on fracture distribution is presented in this study. In this model, the reservoir is simulated using a system of blocks some of which contain fracture zones and fracture-free matrix zones. The fracture distribution is controlled by the stochastic descriptions of fracture density, size, and orientation, which can be obtained from field data. The model is used to simulate an injection operation. Fluid flow, hydraulic potential, and flow rate are calculated, and the stress response is obtained to determine the fracture aperture change for next injection step. Results show that, as expected, the permeability and flow rate increase in response to injection-induced shear slip in the formation. This is also reflected in the wellbore variation with respect to time.

INTRODUCTION

In geothermal system, geothermal energy is extracted from deep and low permeability reservoir by circulating water flow through natural and man-made fracture network contained in the reservoir. Early experimental projects take advantage of pre-existing path ways in the reservoir, such as joints, faults, and nature fractures. However, to make the energy production more economical, reservoir stimulation is used to enhance permeability and heat extraction surface. With interactions between in-situ stresses and injection induced pore pressure, natural fractures in the reservoir start to shear and propagate, thus, enhancing the hydraulic conductivity of the fracture network.

Early practice in this area has shown that for successful engineering of a geothermal reservoir, it is crucial to grasp the mechanical, hydraulic and chemical processes and their interactions in the design process. Thus, an appropriate numerical model of the reservoir stimulation is essential for reservoir development. Previous work in this area includes deterministic modeling of fracture (Kolditz and Clauser 1998, Ghassemi et al. 2007, and Safari and Ghassemi 2011) and stochastic approaches (Bruel 1995, Willis-Richards et al. 1996, and Kohl et al. 1995). These works have neglected certain coupled processes or have considered them using simplifying assumption. In this paper we present results of work in progress on development of a 3D coupled model that utilizes stochastic fracture modeling with the objective of proving flexibility in forward modeling process of geothermal systems and to predict the results of reservoir stimulation and circulation operations.

FRACTURE NETWORK MODELING

In DFN models, series of individual fractures are generated based on stochastic descriptions of fracture density, fracture orientation and fracture diameter. DFN models have been studied for a few decades, for example, by Schwartz et al. (1983), Dershowitz (1988), Cacas et al. (1990), and Willis-Richards et al. (1996). In this study, the approach introduced by Cacas et al., 1990 is adopted. At this stage of our work, the rock mass is considered to be elastic and the fluid flow is treated as an uncoupled transient process governed by diffusion equation (equation 1):

$$c_x \frac{\partial^2 u_w}{\partial x^2} + c_y \frac{\partial^2 u_w}{\partial y^2} + c_z \frac{\partial^2 u_w}{\partial z^2} = \frac{\partial u_w}{\partial t} \quad (1)$$

where c_x, c_y, and c_z are the diffusion coefficients in the x-, y- and z-directions. u_w represents the excess

pore pressure, and t is time. This equation is solved by finite element method using the discrete matrix form:

$$[k_c][u_w] + [m_m]\left\{\frac{du_w}{dt}\right\} = [q] \quad (2)$$

A 3D Finite Element model is developed based on the work of Lee and Ghassemi (2011) to analysis this transient state flow in the fracture network to obtain the injection induced pore pressure. Relationship between fracture aperture change and effective stress variation is established by assuming that the shear dilation occurs when shear strength of the fracture face is exceeded. The new fracture geometry is then substituted into next solution step as the starting point.

STOCHASTIC FRACTURE NETWORKS

The 3D networks of planar, penny-shape fracture in this study are generated follows Cacas et al. (1990). This representation of fracture networks using stochastic methods has met with considerable favor in modelling HDR reservoir simulation in several projects (Bruel et. al 1995 and 2002, Kohl et al. 1995). Fracture clusters are generated throughout the fracture zone based on stochastic description of the fracture center distribution, fracture size (radius) distribution, and fracture orientation (dip and strike). In this study we assume a Poisson distribution for fracture density, log-normal distribution for fracture size, and the Fisher von Mises distribution for fracture orientation as described below (Cacas et al. 1990).

Fracture Density

Fracture density is described using Poisson's distribution. The coordinates of fracture centers (X, Y, and Z) are generated using a random number generator following Poisson's distribution as a 3xN matrix, where N is the number of natural fractures to be generated in the reservoir. The Poisson's parameter lamda (λ) is fixed according to the fracture density. For example, if fracture density is 5 fractures per cubic meter detected from representative field data, and the model size is decided to be 100×100×100 cubic meter, the Poisson's parameter λ for this case is calculated as 5× (100×100×100) and equals to 5,000,000. Poisson's parameter λ represents the expectation of fracture quantity in selected reservoir matrix size. However, if the detected fracture density is described in fracture per unit length, λ should be calculated as density times the length of the model cube. The latter is used in this study.

Fracture Diameter

The distribution of fracture diameter is reported in the lecture to follow the log-normal distribution (Cacas et al. 1990). An array of radius value (r) is first generated randomly according to normal distribution with a mean of zero and a standard deviation of 1. Then, it is transformed to log-normal distribution in the following manner. Given a random variable r drawn from the normal distribution with 0 mean and 1 standard deviation, then the variable R obtained from equation (3) will have a log-normal distribution with parameters μ **mean and** σ standard deviation:

$$R = \exp(\mu + r\sigma) \quad (3)$$

In field detected data, μ is the mean of the log (radius in meters), and σ is the standard deviation of the log (radius in meters). A relation between fracture radius and fracture aperture is introduced by Tezuka and Watanabe (Tezuka and Watanabe, 2000), and be used in this study:

$$a = \alpha\sqrt{r};\ \alpha = 4 \times 10^{-3} \quad (4)$$

Fracture Orientation

The orientation of fracture can be described by its strike and dip (Figure 1). Two angles describing the pole to the plane in spherical coordinates (θ and φ) follow the Fisher von Mises distribution (Cacas et al. 1990):

$$\mathbf{f(\alpha)} = \frac{\mathbf{k}}{\mathbf{2\ sh(k)}} \exp(k\cos(\alpha))\sin(\alpha) \quad (5)$$

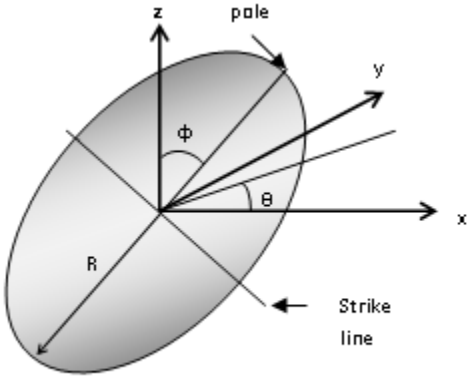

Figure 1: Representation of penny-shape fracture in the model

The CFD (cumulative distribution function) of Fisher von Mises distribution is generated as discrete random numbers U first, and then these random numbers are transferred into random angles following Fisher von Mises distribution by applying the inverse

function of CFD of Fisher von Mises distribution. The process is described as following:

$$U = \int_0^x f(\theta)d\theta = \frac{1}{2}(e^k - e^{kCos[x]})Csch[k]$$

Solving for x from above equation, yields:

$$x = \mathbf{ArcCos}\left[\frac{\mathbf{Log}[e^k - 2U\mathbf{Sinh}[k]]}{k}\right] \quad (7)$$

where x expressed by U are the random angles following Fisher von Mises distribution, and describe the orientation of the fractures. The Fisher von Mises parameter k is from field data.

In summary, the parameters needed from field data to describe the generated fracture network in this DFN model are fracture density, the mean and standard deviation of the log radius in meters, and the Fisher von Mises parameter k. Fisher von Mises parameter k is obtained by conducting statistic study of field gathered fracture orientation data. The number of fractures in the simulated rock cube is a user assigned number that usually is estimated from field. Figure 2 shows a typical fracture network example used in this study that was generated following the stochastic procedure described above.

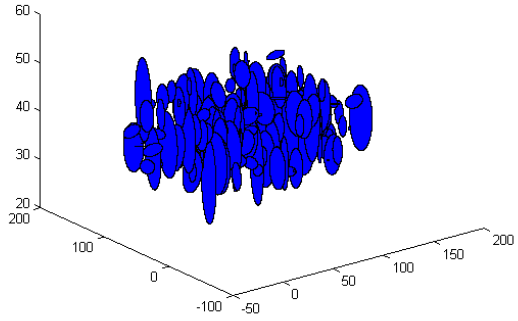

Figure 2: Fracture network generated following stochastic description.

The model used in this study considers a fractured rock block of 15 m thick, sandwiched by two non-fractured rock layers, an injection well is set up and water is pumped only into the fractured layer, thus setting up a 3D flow in the body as shown below (Figure 3).

To discretize the domain, an axisymmetric finite element mesh is created for this reservoir model (Figure 4), having a finer mesh for the near wellbore area, and a coarser mesh with larger elements for the far-field. As can be seen in Figure 4, eight-node brick elements are used. There are totally 10350 elements and 11904 nodes in the mesh. The simulated domain is discretized into 30 horizontal layers and 16 vertical layers.

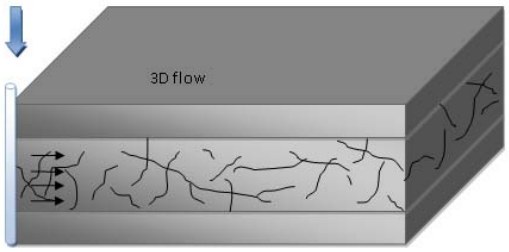

Figure 3: Schematic description of stimulated body

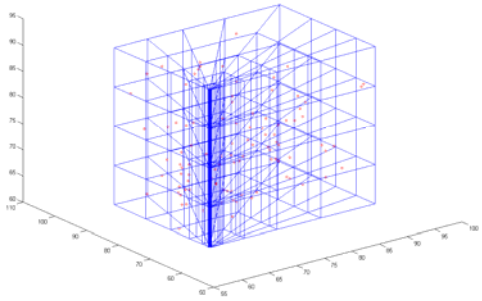

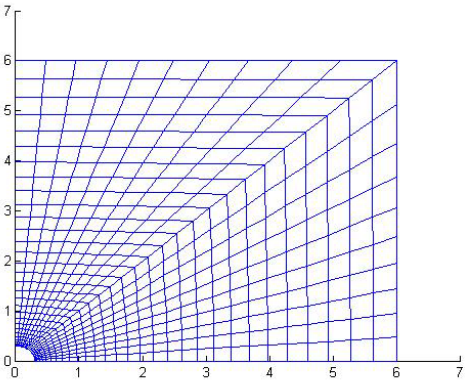

Figure 4: Top: 3D view of one quarter of the Finite Element Mesh with fracture centers. Bottom: Top view of ¼ of the finite element mesh.

FRACTURE FLOW MODEL

The flow model is based on the assumption that fluid moves through the reservoir body within an interconnected fracture network, and that flow in the rock matrix is negligible in comparison with the flow in the fracture. The water flow in fracture is assumed to be governed by the cubic law (Zimmerman and Bodvarsson, 1996) shown by the following equation:

$$Q = \frac{w a^3}{12\mu} \frac{\Delta p}{\Delta L} \quad (8)$$

where Q is the volumetric flow rate in m^3/s, w is the length of intersection line between fracture and element interface in m; a is the aperture of the fracture in m; μ is the fluid viscosity; Δp is the pore pressure change in Pa after the flow travel through ΔL distance in m. By manipulating the geometric relations, the intersection line between the penny-shape fracture surface and the element interface plane can be obtained, as shown in Figure 5. After collecting all the intersection line lengths and related fracture apertures, the permeability term in the above cubic law is be obtained as the equivalent permeability on the element interface. The average element permeability along (x, y, and z) coordinates can then be expressed as the following equation:

$$K_l = \frac{1}{6} \sum_{m=1}^{6} K_m \, n_{ml}$$
$$l = x, y, z; \; m = 6 \; interface \; of \; the \; element \quad (9)$$

Where K_x, K_y, and K_z are element permeabilities along coordinates directions; K_m *(m=1, 6)* are the equivalent permeability on six element interfaces; and n_{ml} represents the projection of the normal on the m^{th} interfaces to the l coordinate (Figure 5). After multiplying by the interface normal cosines, they are projected to normal directions, and then the average local permeability of an element can be obtained.

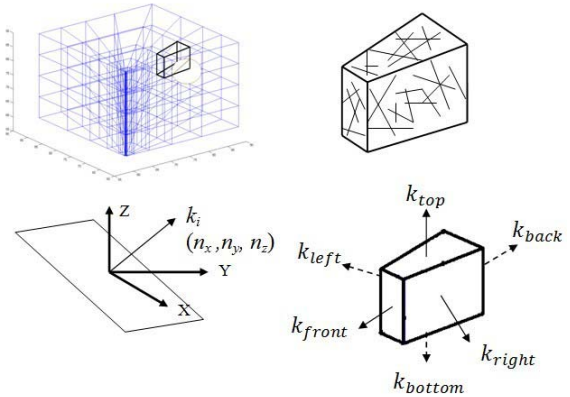

Figure 5: Detecting intersection lines of fracture and element planes, and converting fracture permeability to equivalent local values at the element interface.

INJECTION INDUCED STRESSES AND FRACTURE RESPONSE

As a result of the fluid injection, an incremental pore pressure will be developed throughout the stimulated rock mass. The pore pressure is determined through a 3D transit flow simulation. The fracture response to the combined effects of injection induced pore pressure and in-situ stress is analyzed with respect to permeability enhancement. In this procedure, the effective stress is defined by:

$$\sigma_{eff} = \sigma_{total} - p \quad (10)$$

The normal and shear stresses at fracture center (Figure 6) are then calculated.

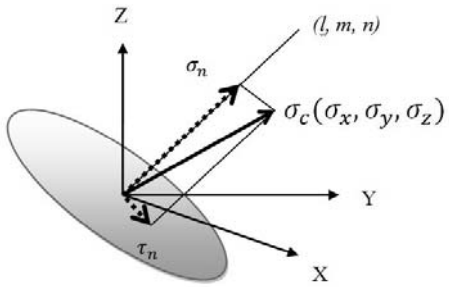

Figure 6: Schematic for calculation of normal and shear stresses at fracture center.

Fracture Aperture

The "in contact" fracture aperture is given by (Willis-Richards et al. 1996)

$$a = \frac{a_0}{1 + \frac{9\sigma_{eff}}{\sigma_{nref}}} + a_s + a_{res} \quad (11)$$

where a_0 is the initial fracture aperture; a_s the change in aperture due to shear dilation; a_{res} is the residual aperture when effective stress is zero ($\sigma_{eff} = 0$). σ_{nref} is the effective normal stress applied to cause a 90% reduction in the compliant aperture (Willis-Richards et al. 1996). The shear slippage criterion can be derived from the linear Mohr-Coulomb failure criterion, that is, the shear slippage occurs when the shear stress exceeds the shear strength:

$$\tau_n \geq \sigma_{eff} \tan\varphi \; ; \; \varphi = \varphi_{basic} + \varphi_{dil}^{eff} \quad (12)$$

where φ_{basic} is material property, basic friction angle, can be measured from lab test. The effective shear dilation angle φ_{dil} can be written in terms of measured shear dilation angle φ_{dil}:

$$\varphi_{dil}^{eff} = \frac{\varphi_{dil}}{1 + \frac{9\sigma_{eff}}{\sigma_{nref}}} \quad (13)$$

Shear slippage will result in a shear displacement which will significantly affect the permeability of the fracture. According to linear elastic theory, the shear displacement U_s can be calculated as:

$$U_s = \frac{\Delta\tau_n}{K_s} \tag{14}$$

where $\Delta\tau_n$ is the excessive shear stress which provide shear slippage, and it can be calculated as the difference between shear stress and shear strength:

$$\Delta\tau_n = \tau_n - \sigma_{eff} \tan\left[(\varphi]_{basic} + \varphi_{dil}^{eff}\right) \tag{15}$$

The change in fracture due to accumulated shear can be expressed as:

$$a_s = U_s \tan\left(\varphi_{dil}^{eff}\right) \tag{16}$$

The total aperture after the shear can be obtained as

$$a = \frac{a_0}{1 + \frac{9\sigma_{eff}}{\sigma_{nref}}} + a_s = \frac{a_0 + U_s \tan(\varphi_{dil})}{1 + \frac{9\sigma_{eff}}{\sigma_{nref}}} \tag{17}$$

CASE STUDY

Numerical experiments are conducted based on Finite Element Method using data provided in the following table (Table 1), and the model geometry is described in Figure 8 and Table 1.

Model Formulation

The equation in element level from equation (2) for the transient flow calculation in this study is given by

$$[k_c][p] + [m_m]\left\{\frac{dp}{dt}\right\} = \{q\} \tag{18}$$

where [$\boldsymbol{k_c}$] represents the permeability or conductivity matrix, [$\boldsymbol{m_m}$] represents the element mass matrix, [$\boldsymbol{p}$] represents the pore pressure matrix, and [$\boldsymbol{q}$] represents the injected flux, that is the source term in this material balance equation.

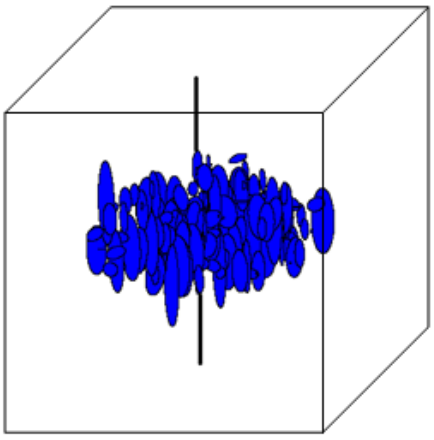

Figure 8: Geometry of studied reservoir model

If an element assembly method and Crank-Nicolson method are to be used, the following equation represents the global situation can be obtained.

$$\left([M_m] + \frac{\Delta t}{2}[K_c]\right)\{P\}_1 = \left([M_m] - \frac{\Delta t}{2}[K_c]\right)\{P\}_0 + \{Q\}$$

where [$\boldsymbol{K_c}$], [$\boldsymbol{M_m}$], {$\boldsymbol{P}$}, and {$\boldsymbol{Q}$} represents the global counterparts of [$\boldsymbol{k_c}$], [$\boldsymbol{m_m}$], {$\boldsymbol{p}$}, and {$\boldsymbol{q}$}. Δt represents a assigned fixed time step and two consecutive time steps are represents as "0" and "1" in the above equation. If some pre-processed manipulation is made on the above equation, it can be written as an equation which is more easily to be handled:

$$[K]\{P\}_1 = [B]\{P\}_0 + \{Q\} \tag{20}$$

where [**K**] replaces $\left([M_m] + \frac{\Delta t}{2}[K_c]\right)$, and [**B**] replaces $\left([M_m] - \frac{\Delta t}{2}[K_c]\right)$. Within each time step, the right hand side terms are known and can be computed, followed by forward and backward substitution, the left hand side pore pressure matrix $\{\mathbf{P}\}_1$ can be obtained. One point need to be pay attention in model formulation is the assembly of the hydraulic conductivity matrix. The hydraulic conductivity or permeability terms in matrix [$\boldsymbol{K_c}$] used in equations above is not the same as typical nomenclatures used in Darcy's law or diffusive equation but we still call this complicated term obtained from math-manipulation permeability matrix in the context.

Table 1: Model parameters (Rahman et al. 2002, Tezuka et al. 2005, and Cacas et al.1990)

Rock properties	
Young's modulus(GPa)	40
Poisson's Ratio	0.22
Density(kg/m^3)	2700
Fracture basic friction angle(deg)	40
Shear dilation angle(deg)	3.0
90% closure stress (MPa)	20
In situ mean permeability (m^2)	6 x 10 $^{-17}$
Fracture properties	
Fracture density(m^{-1})	1.5
Fisher parameter	3.4
Mean fracture radial (lognormal)	0
Standard deviation of fracture radial	0.7
Stress state	
Vertical stress (MPa)	62
Maximum horizontal stress (MPa)	78.5
Minimum horizontal stress (MPa)	63.7
Fluid properties	
Viscosity(N s/m^2)	3 x 10 $^{-4}$
Hydrostatic fluid pressure (MPa)	32
Other reservoir data	
Number of wells	1
Well radius (m)	0.15
Netpay (fractured layer) thickness (m)	15
Model size(m^3)	75*75*75

RESULTS

To verify the numerical model, experiments are performed as follows. First of all, a one stage injection experiment is performed to compare with the analytical solution from Lee et al. 2003 (Figure 9). After that, an isotropic and homogenous porous media with a uniform permeability of $3x10^{-7}$ m^2 containing no fractures is tested with a three-stage injection (Figure 10). All other parameters, such as field stress state, initial pore pressure, model size and so on are held same as described in Table 1. Figure 10 shows the pressure record for the three stage injection test. The curve is similar to a typical transient flow test curve and shows the appropriate variation with the change of injection rate.

In the third test, the stochastic fracture network is added to the model, and the equivalent permeability of the reservoir is obtained in three coordinate directions. The rock matrix permeability in this case is set to be $3x10^{-17}$ m^2, which indicates a low permeability rock in the reservoir. A series of 200 fractures following the statistic distribution described previously is introduced into the rock matrix. The fracture density is 1.5 m^{-1}, which forms a highly fractured rock mass. Other parameters are the same as described in Table 1. No permeability enhancement is allowed in this case. To portray the conductivity of the reservoir and to show the development of the wellbore pressure curve in a relatively short time period, different levels of injection rates were tried out to find an appropriate range for the model parameter set used. Normally, this would be done by the model itself. The wellbore pressure result is shown in Figure 11. In this case, the fracture network is converted to an equivalent permeability of the reservoir. This manipulation approximately simulates the flow between two elements, and thus the accuracy of this method partially depends on the mesh size of the finite element model. In this study, element size of *0.01 m x 0.15 m x 3.2 m* is used in near wellbore area, and element size of *0.6 m x 3.8 m x 3.2 m* is used in far field, as can be seen in previous discussion (Figure 4).

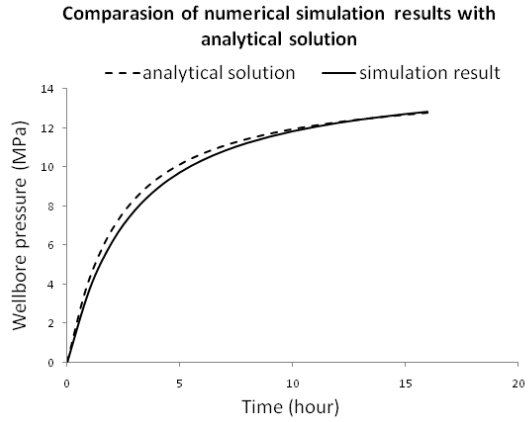

Figure 9: Comparison of numerical solution with analytical solution.

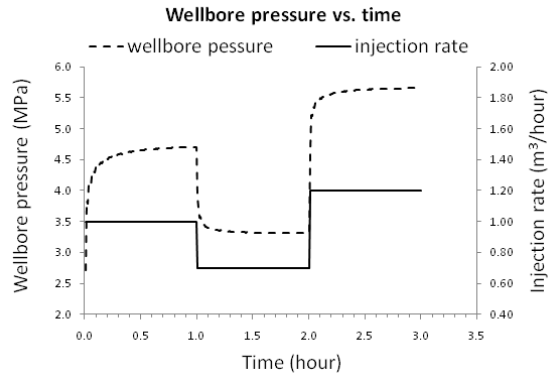

Figure 10: Wellbore pressure change with time in an isotropic homogenous porous rock.

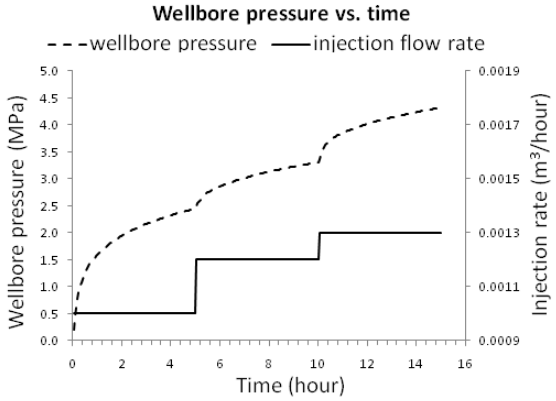

Figure 11: Wellbore pressure development with time in a naturally fractured reservoir.

To simulate the injection induced permeability enhancement, a shear slippage criterion was introduced, as discussed previously. In order to make certain the injected flow opens the existing fracture noticeably, and hence to obtain a good stimulation result, a larger injection rate, 0.075m^3/hour, is applied. A small time step of $\Delta t =$ 0.05 hour is used here to make the equation solving process in finite element analysis stable. The small time step is also essential to make the model more accurate, due to the uncoupled process is assumed in this study. One experiment was used to illustrate the permeability enhancement by the fluid injection. Figure 12 shows the wellbore pressure curves for a stimulation job using an injection rate of 0.075m^3/hour. The dashed line is for the case of no stimulation and is obtained by assuming the fractures are very strong in shear. This assumption is made only to show the comparison between the no stimulation case and stimulated case. The solid line shows the wellbore pressure for the stimulated case. From Figure 12, it can be seen that the wellbore pressure drops as the stimulation proceeds. It should be noticed that before the wellbore pressure drops, it slightly increases with a peak. To address this situation, the stimulated aperture expression is examined (Equation 17), it can be shown that at early shear stage, the stimulated aperture might actually drop below its initial fracture aperture. When shear induced aperture change satisfied the following equation, the stimulated aperture will be greater than the initial aperture of the fracture.

$$\frac{a_0}{1+\frac{9\sigma_{eff}}{\sigma_{nref}}} + a_s > a_0$$

$$thus, \qquad a_s > a_0\left(\frac{9\sigma_{eff}}{\sigma_{nref}}\right) \qquad (21)$$

A jump of wellbore pressure is also shown up in later test, as can be seen in Figure 13.

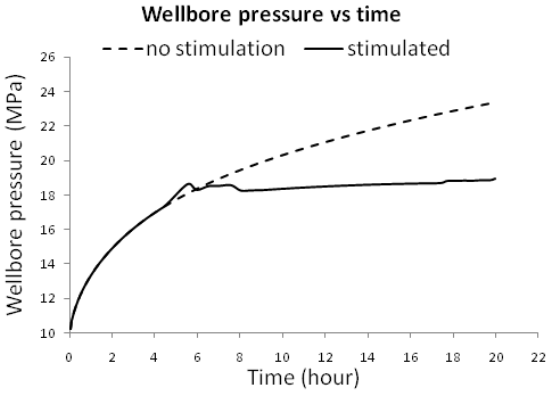

Figure 12: Wellbore pressure profile of a single-stage injection test on naturally fracture reservoir.

As can be predict from the analytical solution of the radial flow equation, for a fixed injection rate in a constant permeability rock, the rate of increase of wellbore pressure gradually declines, reaching a stable level (Figure 9).

The results suggest that an effective practice of reservoir stimulation would be better to increase the stimulation rate before the increase rate of wellbore pressure declines. A three-stage stimulation practice is conducted and the wellbore pressure results are shown in Figure 13. In this example the reservoir is stimulated with three injection rates, 0.05m^3/hour, 0.075m^3/hour, and 0.1m^3/hour. In the three stage case, the permeability enhancement also happens when the injection rate is 0.075m^3/hour, as in the previous one stage case. However, 30% less amount of fluid is used in the latter case to get the reservoir stimulated. According to this result, it is not economic to fix the injection rate at very high level from the very beginning of the stimulation, because in this way more energy and fluid is request than multilevel stimulation.

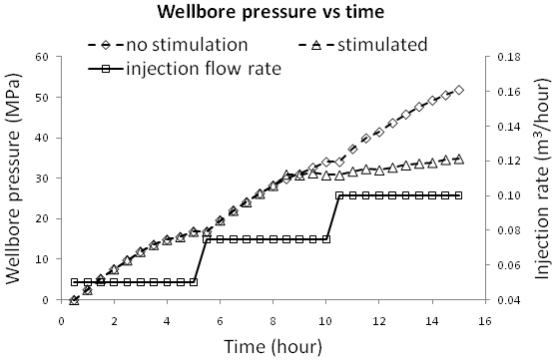

Figure 13: Wellbore pressure profile of a three-stage injection test in naturally fractured reservoir.

Figure 14 and 15 show the flow rates for simulation results of the naturally fractured layer. Figure 14 illustrates the results of the case where fracture aperture improves during injection and Figure 15 shows the case where no fracture aperture improvement is allowed. From these results, it can be noticed that the simulation effect only reach to about 80R (R = 0.15m) from the wellbore in both these cases. In this study, the far field boundary is assumed as a no flow boundary, i.e., there is no outlet for the flow. The injected amount of fluid is assumed to be fully utilized to build up the pore pressure and hence enlarge the fracture aperture. During the early age of the injection, the two flow rate profiles are identical before the aperture is changed at t =5-6 hour. After t = 6 hour, where fracture enlargement is made as shown in Figure 12, some difference in profiles of stimulated and non-stimulation cases are observed. In stimulated case, the flow rate tends to be smaller than in the non-stimulated case. In stimulated case, the permeability is increased while injection rate is fixed. Therefore, flow rate in the stimulated case should be smaller than in the non-stimulated case, as shown. The flow rate profiles also portray the very high heterogeneous nature of the rock mass. A preferential flow channel can be established if a producer is set up, as planned for a future study. The fracture orientation parameter in this simulation is 3.4, and the generated angle data fall between 10.6 – 20 degree range for both fracture strike and pole. As expected, the fracture orientation also affects the flow channel preference during the stimulation.

The average permeability of the reservoir is obtained from a 6-stage stimulation test and shown in Figures 16 and 17. Also, permeability of the 3-stage injection discussed previously (Figure 13) is obtained for comparison. Figure 16 shows again that the permeability is enhanced when the injection rate reach 0.075 m^3/ hour. It can be observed that before the shear stress exceeds the shear strength of the fracture, a decrease in the injection rate would not result in a permeability reduction. However, after stimulation, increase or decrease of the injection rate will affect the calculated permeability of the reservoir.

Figure 17 shows the average reservoir permeability as a function of wellbore pressure for the 6-stage injection, where the average reservoir permeability increases proportionally to the wellbore pressure. The permeability increases rapidly upon achieving a wellbore pressure of 15 MPa, indicating a drastic fracture aperture enlargement.

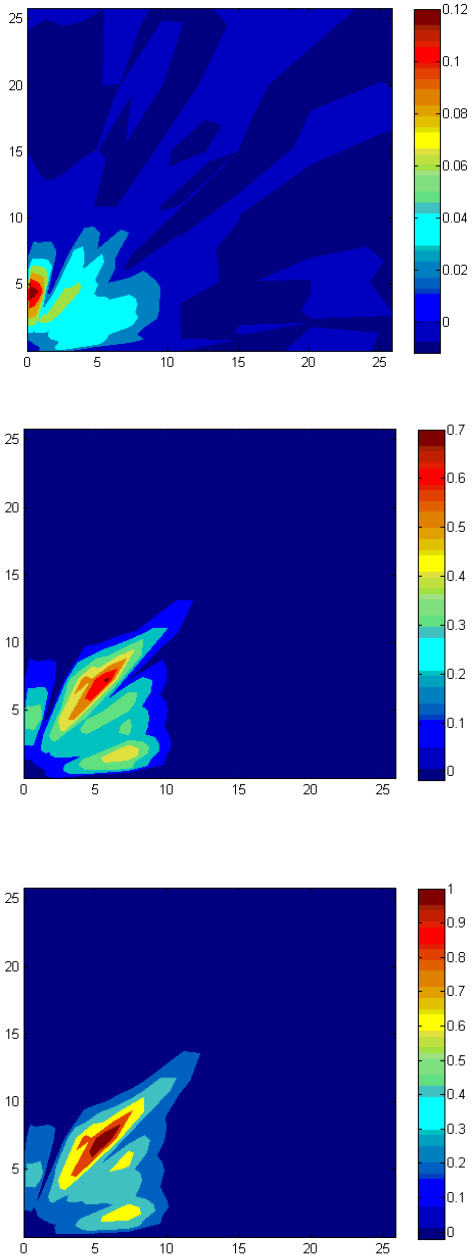

Figure 14: Flow rate profile after t = 2, 12, 20 hours of injection at a rate of 0.075m^3/hour in stimulated fractured zone.

Figure 18 shows the permeability change with injection rate during the 3-stage injection, and the results coincidence Figure 13, that the permeability increases at t=8-10 hour. Figure 19 shows the average reservoir permeability as a function of wellbore pressure for the 3-stage injection. Similar to

the 6-stage injection results (Figure 17), the permeability increases proportionally to the wellbore pressure. By comparing the permeability profiles of these two cases, it can be seen that the permeability change occurs at about the same volume of fluid injected (0.66 m^3 for 6-stage and 0.63 m^3 for 3-stage injection).

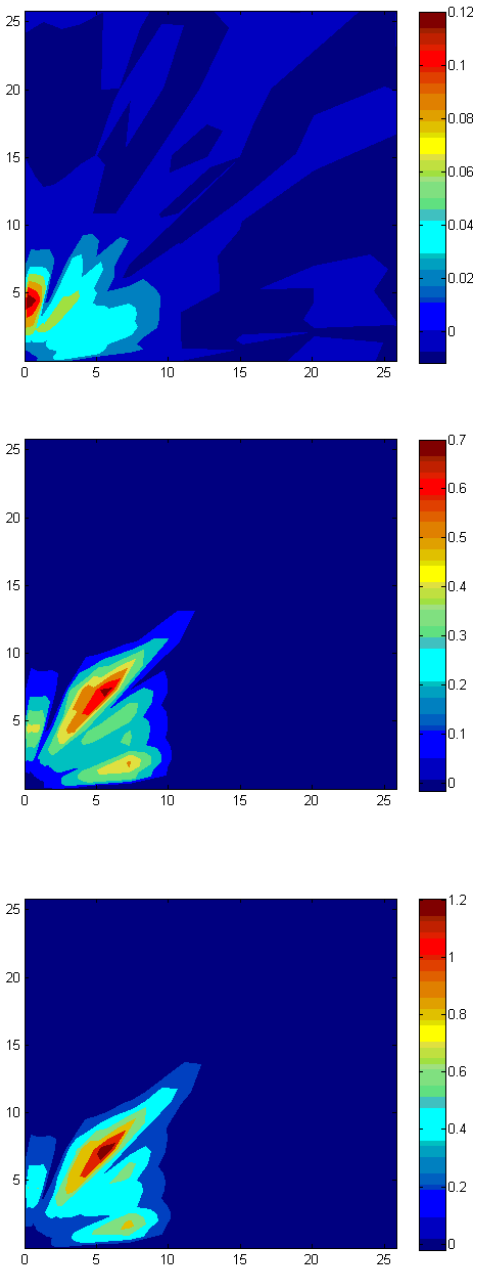

Figure 15: Flow rate profile after t = 2, 12, 20 hours of injection at a rate of 0.075m^3/hour in non-stimulation fractured zone.

However, as can be seen from Figure 17 and Figure 19, the wellbore pressure when the permeability enhancement is observed is higher in the 3-stage injection case than in the 6-stage injection. Figure 20 compares the permeability change with time for the 3-stage injection and 6-stage injection. As expected, the permeability enhancement is observed later in the 6-stage case at lower wellbore pressure. However, it catches up rapidly due to the increase of injection rate from 0.075 m^3/ hour to 0.1 m^3/ hour at t = 15 hour.

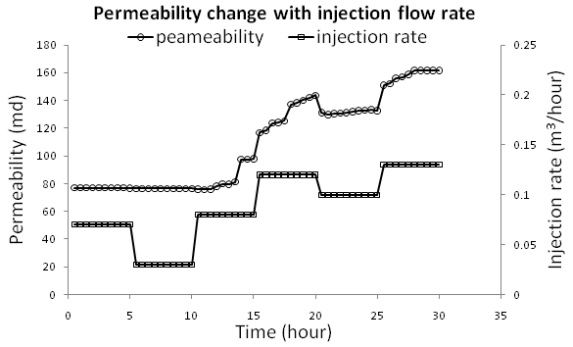

Figure 16: Enhancement of the reservoir permeability (average) during 6-stage stimulation.

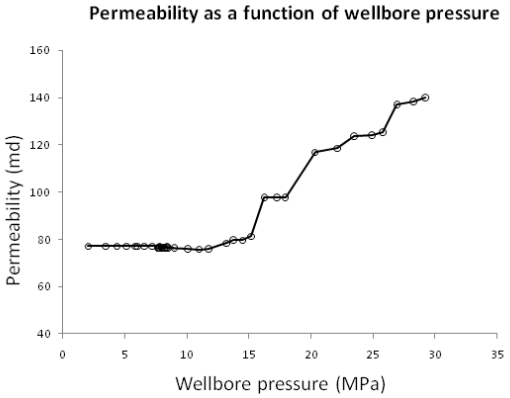

Figure 17: Average permeability as a function of wellbore pressure during 6-stage stimulation.

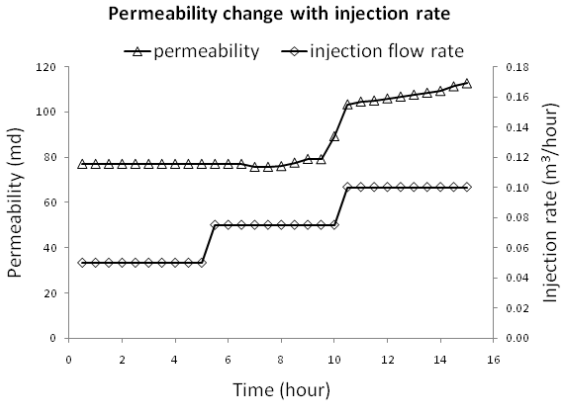

Figure 18: Enhancement of the reservoir permeability (average) during 3-tage stimulation.

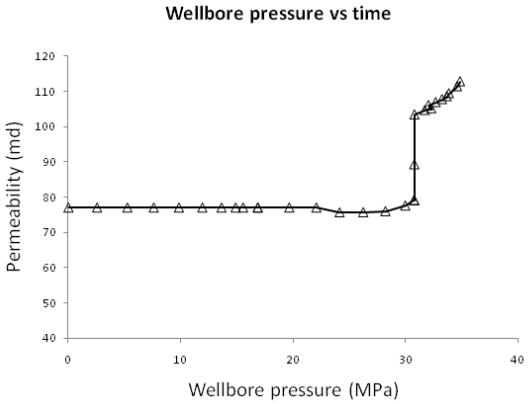

Figure 19: Average permeability as a function of wellbore pressure during 3-stage stimulation.

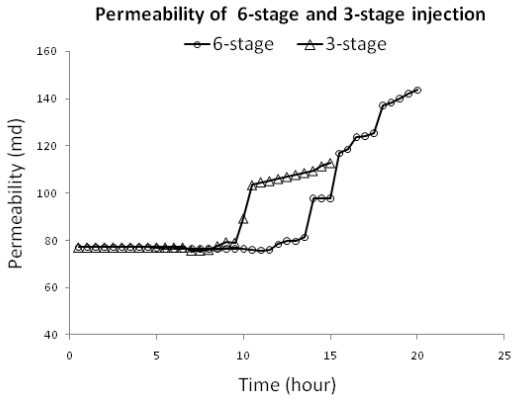

Figure 20: comparison on permeability enhancement of 3-stage and 6-stage injection

CONCLUTION

This paper presents results of work in progress on development of a 3D fully-coupled model for analysis of the thermo-hydro-mechanical response of a geothermal system using a stochastic fracture network. The flow through fractured reservoir is treated as transient flow and equivalent permeability concept is used to evaluate the permeability of fractured blocks. Several numerical experiments have been conducted to verify the model, to evaluate its status and demonstrate its capabilities. The simulation results compare well with the analytical solution of radial flow in porous media. An example for a naturally fractured reservoir illustrates the difference between the wellbore pressure profiles of the stimulated case and non-stimulated case, reflecting the stimulation effect of injection. The average reservoir permeability is enhanced during stimulation, and the flow rate in the formation is increased. For the injection rate and rock data used, the area of permeability improvement is limited to a zone nearly eight times the radius of the wellbore. A preferential flow pathway develops as the injection continues. Results underscore the significance of the orientation of natural fractures and their stimulation on the flow pathway. The improvement on average reservoir permeability is proportional to the wellbore pressure. And the permeability increases rapidly after some critical wellbore pressure. The value of critical wellbore pressure depends on the injection history and fracture properties, and stress state.

REFERENCES

Bruel, D. (1995), "Heat Extraction Modeling from Forced Fluid Flow Through Stimulated Fractured Rock Masse Application to the Rosemanowes HDR Reservoir," *Geothermics*, **24**, 361-374.

Brue.D. (2002), "Impact of Induced Thermal Stresses During Circulation Tests in An Engineered Fractured Geothermal Reservoir; Example of The Soultz-sous-Forets European Hot Fractured Rock Geothermal Project, Rhine Graben, France," *Oil and Gas Scienceand Technology Rev IFP,* **57** , 459–470.

Cacas, M. C., Ledoux, E., De Marsily, G. and Tillie, B. (1990), "Modeling Fracture Flow with A Stochastic Discrete Fracture Network: Calibration and Validation: 1. The Flow Model," *Water Resources Research,* **26(3),** 479-489.

Dershowitz, W. S. and Einstein, H. H. (1988), "Characterizing Rock Joint Geometry with Joint System Models," *Rock Mechanics and Rock Engineering,* **21**, 21-51.

Ghassemi, A., Tarasovs, S., and Cheng, A. H.-D. (2007), "A Three-Dimensional Study of The Effects of Thermo-Mechanical Loads on Fracture Slip in Enhanced Geothermal Reservoir," *International Journal for Rock Mechanics & Mining Science* **44**, 1132–1148.

Kohl, T., Evans, K. F., Hopkirk, R.J., and Ryback, L. (1995), "Coupled Hydraulic, Thermal, and Mechanical Considerations for The Simulation of Hot Dry Rock Reservoirs," *Geothermics*, **24**, 345-359.

Kolditz, O., and Clauser, C. (1998), "Numerical Simulation of Flow and Heat Transfer in Fractured Crystalline Rocks: Application to The Hot Dry Rock Site in Rosemanowes (U.K.)," *Geothermics*, **27**, 1-23.

Lee, J., Rollins, J. B. and Spivey, J. P. (2003), "Pressure Transient Testing," SPE Textbook Series.

Lee, S. H. and Ghassemi, A. (2011), "Three-dimensional Thermo-Poro-Mechanical Modeling of Reservoir Stimulation and Induced Micro-seismicity in Geothermal Reservoir," *Thirty-Sixth Workshop on Geothermal Reservoir Engineering (in press), Stanford University, Stanford, California.*

Rahman, M. K., Hossain, M. M. and Rahman, S. S. (2002), "a Shear-dilation-based Model for Evaluation of Hydraulically Stimulated Naturally Fractured Reservoirs," *Innational Journal for Numerical and Analytical Methods in Geomechanics.*, **26**,469-497.

Safari, M. A. and Ghassemi,A. (2011), "3D Analysis of Huff and Puff and Injection Tests in Geothermal Reservoirs," *Thirty-Sixth Workshop on Geothermal Reservoir Engineering (in press), Stanford University, Stanford, California.*

Schwartz, F. W., Smith, L, and Crowe, A. S. (1983), "A Stochastic Analysis of Macroscopic Dispersion in Fracture Media," *Water Resources Research*., **19(5),**1253-1265.

Tezuka, K. and Watanabe, K. (2000), "Fracture Network Modeling of Hijiori Hot Dry Rock Reservoir by Deterministic and Stochastic Crack Network Simulator (D/SC)," *Proceeding World Geothermal Congress 2000*.

Tezuka, K., Tamagawa, T. and Watanabe, K. (2005), "Numerical Simulation of Hydraulic Shearing in Fracture Reservoir," *Proceeding World Geothermal Congress 2005*.

Willis-Richasrds, J., Watanabe, K. and Takahashi, H. (1996),"Progress Toward A Stochastic Rock Mechanics Model of Engineered Geothermal Systems," *Journal of Geophysical Research*, **101**, 481-496.

Zimmerman, R. W. and Bodvarsson, G. S. (1996), "Hydraulic Conductivity of Rock Fractures," *Transport in Porous Media*, **23**, 1-30.